IJBPAS, April, 2023, 12(4): 1400-1416

ISSN: 2277–4998

International Journal of Biology, Pharmacy and Allied Sciences (IJBPAS)

'A Bridge Between Laboratory and Reader'

www.ijbpas.com

DESIGN AND DEVELOPMENT OF POTENTIAL ANTI-TUBERCULAR LEADS POSSESSING 4-AMINO QUINOLINE MOIETY AS DNA GYRASE B INHIBITORS

VENKATESAN S[1#], PAVITHRA L[1#], HARITHA M[1], APARNA RAM[1], GOPINATH P[2] AND KATHIRAVAN MK[2*]

1: Department of Pharmaceutical Chemistry, SRM College of Pharmacy, SRMIST, Kattankulathur, Chengalpattu, Tamilnadu, India

2: 209, Dr. APJ Abdul Kalam Research Lab, SRM College of Pharmacy, SRMIST, Kattankulathur, Chengalpattu, Tamilnadu, India

[#] Authors contributed equally

***Corresponding Author: Dr. Kathiravan MK: E Mail: drmkkathir@gmail.com**

Received 10th June 2022; Revised 17th July 2022; Accepted 3rd Sept. 2022; Available online 1st April 2023

https://doi.org/10.31032/IJBPAS/2023/12.4.6883

ABSTRACT

DNA gyrase B subunit, a druggable target of potent anti-tubercular agents is involved in the process of ATP hydrolysis which in turn provides energy to gyrase A subunit for maintaining the DNA topological state. In the present study, we employed structural optimization of the reported Gyrase B inhibitors possessing quinoline nucleus employing Quantitative Structure-Activity Relationship (QSAR) and docking studies. QSAR studies were carried out by QSARINS software on 4-aminoquinoline derivatives for the best model having four variables L1i, MoRSEN26, RDFM5 and RDFE25 with statistical values R2 = 0.7430, LOF=0.0608, CCCtr = 0.8525, Q2LOO = 0.6461, Q2LMO = 0.6189, CCCcv = 0.7972, R2ext = 0.8294, and CCCext = 0.8898. The developed QSAR model suggests that the 3D-Weighted Holistic Invariant Molecular descriptors (3D-WHIM), 3D-Molecular representations of structure based on electron diffraction descriptors (3D-MoRSE) and Radial Distribution Function (RDF) descriptors play key roles in predicting bioactivity. The designed compounds using QSAR model predicted molecular descriptor information yielded compounds 42a and 42c as good potential theoretical candidates. Binding energy scores of the designed compounds provided nanomolar activity binding interactions in the active site of 3zkd: DNA Gyrase B enzyme.

Compound 42a, with predicted activity of ~80nM MIC will be take over for further experimental studies as anti-tubercular lead.

Keywords: Anti-mycobacterial activity, Autodock, MoRSE, QSAR

INTRODUCTION

As recorded by WHO (World Health Organization), TB (tuberculosis) which is triggered by Mtb (Mycobacterium tuberculosis) has become one of the deadliest infectious diseases worldwide with a mortality rate of about 1.4 million lives in 2019 **[1]**. While TB may be treated with the frequently used medications like pyrazinamide, ethambutol, rifampicin, and isoniazid, however, it has been noted that treatment of TB is hampered by resistance of *Mtb* to accessible treatments. The failure to comply with treatment regimens has contributed to drug resistance production by a self-supporting mechanism, which resulted in some types of TB by currently accessible anti-tuberculosis medicines being untreatable. The fast development of MDR (multi-drug-resistant) and XDR (extremely drug-resistant) strains of Mtb were identified as an important global treat for control measures for TB **[2]**. So, the current normal MDR-TB treatment needs to be improved to increase patient survival levels.

The DNA topoisomerases act by producing transient local DNA breaks in one or both DNA double helix strands (form I & form II topoisomerases respectively) and moving second DNA segments via the breaks. Form I DNA topoisomerases are independent monomeric ATP enzymes, form II topoisomerases are massive macromolecular devices (heterotetramers or homodimers) using ATP for conducting compliance adjustments in connection with the dual stranded DNA transfer events. Two subunits, GyrB or ParE & GyrA or ParC, for Topo IV and DNA gyrase respectively form the catalytically active heterotetrameric enzymes by bacterial form IIA topoisomerases **[3]**. Topo IV (topoisomerase IV) & DNA Gyrase subunits are similarly functional and systemic and are considered paralogues resulting from an ancestral-type IIA topoisomerase replication gene. ParE & GyrB subunits comprise of two domains, C-terminal Toprim and N-terminal ATPase domain, although ParC & GyrA comprise of the N-terminal BRD (breakage–reunion domain) accompanied by the CTD (C-terminal domain) **[4]**. Though DNA gyrase & Topo IV are homologous, their choice and operation of substrates are remarkably different. DNA gyrase incorporates a right-hand wrap in the DNA that leads to the

insertion of negative supercoils after stranding, thus helping to under wind the bacterial genomes. Topo IV, on the contrary, relieves DNA supercoils preferably, is more optimistic than negative, and has a robust DNA decatenase **[5]**. Bacterial DNA gyrase, as well as Topo IV, are the target of the larger family of antibiotics, the fluoroquinolones, besides playing an important role in cellular effects including transcription, replication, as well as recombination.

Fluoroquinolones targeting at the gyrase A subunit faced a big hurdle of Mtb's resistance that made the Gyrase B subunit druggable for finding powerful anti-tubercular agents **[6]**. DNA gyrase B subunit is included in the ATP (adenosine triphosphate) hydrolysis mechanism which in turn gives power to the gyrase A subunit for keeping the state of DNA topological **[7]**. These antibiotics form the backbone of many therapies for diseases, including multi-drug-resistant tuberculosis with large pathogens. For this cause, TB research focuses on inhibitors that are targeted to different steps. TMC207 (diarylquinoline), an antitubercular drug in Phase II trials acts by inhibiting the enzyme mycobacterial ATP synthase. Importance of many quinoline and quinolone series being prescribed in combination with the first-line and second-line anti-mycobacterial drugs, shows light onto exploration of better compounds **[8]**.

A quantitative correlation between structure and activity which plays a crucial role in optimizing leads and thus improve their biological activity is one of the fair as well as effective approaches in drug design **[9]**. In this context, we have developed leads using molecular modeling studies on nitro imidazooxaazine derivatives as potent anti-tubercular agents acting on polyketide synthase 13 enzyme in the mycolic acid pathway of mycobacterium tuberculosis **[10]**. We explore further augmenting the probability of finding new quinoline-based antimycobacterial leads. Recently we have reported thoroughly validated in-silico studies on triazole benzene sulphonamide as carbonic anhydrase IX inhibitors **[11]**, pyrazole benzenesulfonamide as cyclooxygenase 2 inhibitors **[12]**, and thiochromene derivatives as steroidal sulfatase inhibitors **[13]**.

In continuation to work in the identification and development of novel leads using QSAR, molecular docking tools, we herein report a series of novel 4-aminoquinoline derivatives as inhibitors of Mtb DNA gyrase B. The dataset was taken for QSAR study to predict the function of biological activity substitutes by producing efficient models that can estimate bioactivities with extensive software

parameters. We were also interested in investigating the structural features in optimizing the lead for the Mtb DNA gyrase B inhibition.

MATERIALS AND METHODS

"QSARINS" enables the creation of many linear regression models, carefully checked & validated as per the chemometric method by ordinary fewer squares. The literature reported was based on a sequence of 46 compound data sets (Table 1) of 4-aminoquinoline derivatives with Mtb gyrase B inhibitor values **[14]**. MIC values have been translated and used as a dependent variable to the corresponded pMIC.

Table 1: Dataset compounds with Mtb Gyrase B inhibitory activity

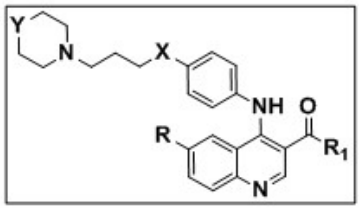

Sl. No	R	R1	X	Y	MIC (µM)	pMIC
1	H	OC2H5	O	O	28.7	4.542118
2	OCH3	OC2H5	O	O	13.35	4.874519
3	F	OC2H5	O	O	21.72	4.66314
4	CF3	OC2H5	O	O	43.1	4.365523
5	H	OC2H5	NH	O	14.38	4.842241
6	OCH3	OC2H5	NH	O	23.36	4.631527
7	F	OC2H5	NH	O	13.45	4.871278
8	CF3	OC2H5	NH	O	49.75	4.303207
9	H	OC2H5	O	NC2H5	13.51	4.869345
10	OCH3	OC2H5	O	NC2H5	11.58	4.936291
11	F	OC2H5	O	NC2H5	3.25	5.488117
12	CF3	OC2H5	O	NC2H5	2.94	5.531653
13	H	OC2H5	NH	NC2H5	6.77	5.169411
14	OCH3	OC2H5	NH	NC2H5	25.43	4.594654
15	F	OC2H5	NH	NC2H5	13.03	4.885056
16	CF3	OC2H5	NH	NC2H5	1.47	5.832683
17	H	NHNH2	O	O	2.4	5.619789
18	OCH3	NHNH2	O	O	55.37	4.256725
19	F	NHNH2	O	O	28.44	4.54607
20	CF3	NHNH2	O	O	36.38	4.439137
21	H	NHNH2	NH	O	44.86	4.348141
22	OCH3	NHNH2	NH	O	27.75	4.556737
23	F	NHNH2	NH	O	23.56	4.627825
24	CF3	NHNH2	NH	O	25.59	4.59193
25	H	NHNH2	O	NC2H5	13.93	4.856049
26	OCH3	NHNH2	O	NC2H5	11.63	4.93442
27	F	NHNH2	O	NC2H5	3.34	5.476254
28	CF3	NHNH2	O	NC2H5	11.51	4.938925
29	H	NHNH2	NH	NC2H5	13.49	4.869988
30	OCH3	NHNH2	NH	NC2H5	13.09	4.88306
31	F	NHNH2	NH	NC2H5	3.3	5.481486
32	CF3	NHNH2	NH	NC2H5	30.03	4.522445
33	H	OH	O	O	30.68	4.513145
34	OCH3	OH	O	O	57.14	4.24306
35	F	OH	O	O	14.69	4.832978
36	CF3	OH	O	O	13.15	4.881074
37	H	OH	NH	O	7.69	5.114074

38	**OCH3**	**OH**	**NH**	**O**	**28.64**	**4.543027**
39	**F**	**OH**	**NH**	**O**	**29.46**	**4.530767**
40	**CF3**	**OH**	**NH**	**O**	**6.59**	**5.181115**
41	**H**	**OH**	**O**	**NC2H5**	**27.19**	**4.565591**
42	**OCH3**	**OH**	**O**	**NC2H5**	**3.3**	**5.481486**
43	**F**	**OH**	**O**	**NC2H5**	**6.91**	**5.160522**
44	**CF3**	**OH**	**O**	**NC2H5**	**19.75**	**4.704433**
45	**H**	**OH**	**NH**	**NC2H5**	**11.8**	**4.928118**
46	**OCH3**	**OH**	**NH**	**NC2H5**	**3.48**	**5.458421**

Molecule structure preparation and 3D geometry optimization

ACD/lab chem sketch freeware 2017.2.1 **[15]** was used to draw referred molecular structures and translate them to a "Sybyl mol2" format utilizing the "Open Babel V2.4.1" **[16]**. The "Avogadro V1.2.0" **[17]** geometry for the addition of hydrogen was optimized by the molecules. MMFF94, the force field of molecular mechanics, and the steepest descent algorithm were used. A genetic algorithm with the energy measurement feature is derived from the avogadro tool for each compound, and the same conformer has been used for the entire study.

Data setup

Fore mentioned compounds were determined for molecular descriptor rates of the online padel tool of "chemdes-chemopy" servers **[18]**. The variables were arranged as well as pre-filtered without all-zero, constant and missing value (>50%) descriptors. The pairwise relationship is utilized to strip out above 0.85 values of descriptors. 3D WHIM, MoRSE, and RDF descriptors demonstrate stronger correlation towards activities by the correlation matrix developed for all filtered descriptors and therefore selected for this analysis. A total of 32 variables with a correlation value above 0.36 have been chosen for the analysis from the testing of descriptors. Forty-six molecules were classified into a 5:1 ratio of preparation and estimation dependent on reaction order. We only show the best model from several trials and models produced.

Model calculation and variable selection

"QSARINS" program examines every user choice identified mixtures of selected descriptors **[19, 20]**. The genetic algorithm is used to assess the fitness of models in descriptor selection relating to molecule's biological activities with the LOF (lack of fit) function of Friedman's. The default degree of LOF smoothness is 1.0. User-defined parameters such as mutation probability (0.1), size of population (200) as well as maximum generations (5000) explore more combinations along with genetic algorithm.

Model validation

The "QSARINS" systems are rigorously validated both external as well as internal and are often checked in the model's applicability domain. Internal validation with Q2LMO (cross-validation leave-many-out), Q2 LOO (cross-validation leave-one-out), RMSE (root mean squared error), external validation, and Y-Scrambling with Q2F1, Q2F2, Q2F3, and CCC (concordance correlation coefficient) were applied on selected models. Q2 LMO is replicated 5000 times with 30 percent items per time left at random as by the training set. Y-scrambling through 5000 iterations process contains response data shifting, to exclude risk relation in the initial model. It is noted that Q2loo & R2 of the model should be comparatively larger than scrambled ones as well as RMSE of the model under prediction should be comparatively smaller than scrambled ones. The CCCext is evaluated to determine model reproducibility. The applicability domain is a conceptual area of descriptive modelling, and the leverage analysis assesses it. The leverage (hat) is measured with hi = xi (XT X)-1 xTi (i=1, 2,…m), here xi indicates the query compound descriptor row-value, i and m denotes the number of query compounds. X represents n x p training set matrix, here n signifies a number of training set samples and p indicates a number of model descriptors. The model domain limit, cut-off value of leverage, h* indicates 3(p+1)/n. Leverage more than h* for the training set implies that the sample is extremely important for the model determining, while the test range (X outliner) the projection is a model extrapolation. Any compound of more than 3σ units residual standardized is recognized as a Y outlier.

Molecular docking studies

The interactions and affinities of the Mtb gyrase B inhibitors were estimated with Autodock V4.2.6 in conjunction with the developed QSAR model **[21]**. The original configuration of the 3D structure of the Mtb GyrB ATPase domain, pdb id: 3ZKD is found by the protein data bank (www.rcsb.org). Using the Modeller V9.23 program **[22]** missing residues were fixed along with the addition of hydrogen atoms and removal of existing ligands. Redocking co-crystallized ligand on 3ZKD was performed to find docking parameters that would be useful for the docking of compounds. The ACD chemsketch 2017.2.1 design was used for all ligand structures and the force field "MMFF94", the steepest descent algorithm with a parameter of convergence fix at 10e-7, was used to optimize the geometry by Avogadro V1.2.0. Open Babel V2.4.1 is used as needed to convert file formats. Geometrically incorporating polar

hydrogens made the protein, and the pdbqt file was allocated to Kollman's unified atomic charges. Histidine residue protonation states were discussed when the ND1 condition was assigned to histidines attached to zinc and NE2 to the rest of the histidines. Ligand preparation is achieved with the inclusion of polar hydrogens by incorporating gasteiger charges. Ligands have defined torsions and pdbqt files are produced. Autogrid alternative allows an active site selection along with grid size to "60*60*60 points" with an interval of "0.375 Å" and a dielectric constant distance-related function has been utilized for the energetic map measurement. The grid box contains the active binding enzyme site with an adequate area of the ligand translational and rotational walk. The genetic algorithm of Lamarckian was used to examine conformation positions within Mtb gyrase B's active site orientation. The parameters were optimized as follows; the maximum amount of energy estimates was raised to "25,000,000" per run. In the population, there were 150 candidates and the highest generation number was 2700 with a 0.02 gene mutation rate. Each other parameter has been set to default. Outcomes in a positional RMSD varying from <2 Å were grouped together. The group representative was chosen for each group as the lowest binding energy configuration with the greatest percentage frequency. The "Discovery Studio Visualizer 2020 version 20.1.0.19295" **[23]** program developed and illustrated presentations of interactions and ligand poses in the figure.

RESULTS AND DISCUSSION

Model information

A dataset of 46 molecules from quinolone series with inhibitory activity were considered for the study. The molecules were optimized for geometry by using MMFF94. Approximately 3000 descriptors were calculated using Padel, Chemopy-chemdesc, RDKit and Bluedesc server. The dataset was divided into training and test based on their chemical and biological diversity and several QSAR model equations were generated using QSARINS. Some of the models showed higher R2 and Q2LOO values but their external validation was not good and they also showed a good number of outliers. QSAR model applicability depends on cross validated presentation (i.e.) robustness and external predictive ability **[24]**. The developed model with aforementioned options gave statistical parameters as,

Final Model:

pMIC = 2.8063 + 0.0475 (L1i) + 3.3770 (MoRSEN26) + 0.0456 (RDFM5) + 0.0394 (RDFE25)

ntr = 34, npred = 06, R2 = 0.7430, R2adj = 0.7075, R2-R2adj = 0.0355, LOF = 0.0608, RMSEtr = 0.1886, MAEtr = 0.1559, RSStr = 1.2096, CCCtr = 0.8525, s=0.2042, F=20.9550, Q2LOO = 0.6461, Q2LMO = 0.6189, R2Yscr = 0.1226, Q2Yscr = -0.2213, RMSEcv = 0.2213, MAEcv = 0.1842, PRESScv = 1.6655, CCCcv = 0.7972, R2ext = 0.8294, MAEext = 0.1417, PRESSext = 0.1590, RMSEext = 0.1628, CCCext = 0.8898, Q2F1 = 0.7550, Q2F2 = 0.7488, Q3F3 = 0.8086.

The final model shows good fitting values along with internal and external validation values. Compared with previous models, the final model shows no outliers in William's plot with increment in external validation parameter values. The scatter plot shown as the experimental versus the calculated Mtb gyrase B inhibitory activities of 4-aminoquinolines is displayed in **Figure 1(left image)**, showcasing predicted values comparable to corresponding experimental values. The inter-correlation among descriptors and response resulted Kxy versus Q2LMO of final model were displayed in **Figure 1(right image)** explaining the LMO parameter values were around the model parameters, determining the final model is robust and stable.

The Y-scramble plot resulted Kxy versus R2Yscr and Q2Yscr, display correlation coefficients of the final model are much higher than those after endpoint scrambling and the structure-response relationship is broken, which can be noticed in **Figure 2 (left)**. Standardized residuals versus leverage values shown in the Williams plot of **Figure 2(right)** illustrate the prediction and express the applicability domain of the model. It is noticed that all the molecules are in the applicability domain of the model with leverage values lower than the warning h^* of 0.441. With the threshold of >0.70, the values of Q2F1, Q2F2 and Q2F3 were found and CCC parameter values were found to be >0.80. The results declare the final model obtained is not by probability and in fact there is an association between structures of 4-aminoquinolines analogs with corresponding Mtb gyrase B inhibitory activity.

Molecular descriptors information

WHIM descriptors **[25]** are based on molecular indices that correspond to diverse sources of chemical information. WHIM descriptors resembling L1i, 1st component size directional WHIM index / weighted by relative first ionization potential, hold information concerning the molecular structure in stipulations of size, shape, symmetry and atom distribution. From a spatial conformation of minimum energy, within different weighting schemes

in a straightforward manner, the index values were calculated. The WHIM descriptor moves toward interaction scalar fields: G-WHIM (grid-weighted holistic invariant molecular) descriptors which are defined and calculated from the grid-points where field interaction energy between the probe and molecule has been evaluated.

The WHIM descriptor algorithm performs principal component analysis by using a weighted covariance matrix **S** on the centered molecular coordinates obtained from diverse weighting schemes for the atoms. The covariance matrix along with elements were denoted as,

$$s_{jk} = \frac{\sum_{i=1}^{n} w_i (q_{ij} - \bar{q}_j)(q_{ik} - \bar{q}_k)}{\sum_{i=1}^{n} w_i}$$

Where *n* is the no. of atoms, *wi* the weight of the *i*-th atom, *qij* denote the *j*-th coordinate (*j* = 1, 2, 3) of the *i*-th atom and qj^{-} is the average of the *j*-th coordinates. Weighting schemes by six ways have been proposed: (1) atomic masses **M** (*wi* = *mi*), (2) the unweighted case **U** (*wi* = 1, *i* = 1, *n*, where *n* is the number of atoms for each compound), (3) the Mulliken atomic electronegativities **E** (*wi* = *elni*), (4) the van der Waals volumes **V** (*wi* = *vdwi*), (5) the electrotopological indices of Kier and Hall S (*wi* = *Si*) and (6) the atomic polarizabilities **P** (*wi* = *poli*).

Structure activity relationship of dataset compounds

Utilizing molecular descriptors information obtained from QSAR studies, a self explorative study on the dataset was performed to identify the model efficiency and accuracy. Residuals from the difference calculated between experimental and predicted bioactivity values were almost near to zero, meaning validated model generation and effective prediction **(Table 2)**. Further using structure function relationship values from dataset, meaningful information was depicted. Substitutions on R1 position of quinoline ring with ethoxy, R position with trifluoromethyl, X with amino and Y with ethylamino groups lead to best-predicted activity as depicted in compound 16. Substitution of amino group of X with oxygen atom resulted in the loss of activity, except in case of methoxy substituent at R position of compound 10. Replacing alkyl amino group at Y position to oxygen group leads to diminished activity as seen in compound 4 and 8.

Substitution on R1 position of quinoline ring with hydrazine group, R position with trifluoromethyl, X with amino and Y with ethylamino groups lead to decreased activity as depicted in compound 32. Replacing amino group of X position to oxygen group and alkyl-amino group at Y position to oxygen group leads to loss of activity as seen in compound 20.

Substitution on R1 position of quinoline ring with hydroxyl group, R position with methoxy, X with oxygen and Y with ethylamino groups lead to increased activity as depicted in compound 42 compared to compound 46. New compounds were designed with varying substituents on the core structure and molecular descriptor values were calculated from online padel tool of chemdes - chemopy servers. **(Table 3)** display predicted activities of best designed compounds from the QSAR final model. The best activity compounds from the original dataset (11, 12, 16, 17 and 31) and the designer series (60 and 61) were selected for molecular docking studies to predict favourable H-bonds interactions and binding scores.

Molecular docking studies

H-bond interactions were seen in compound 11 with the residues Asn309, Trp47, Thr371, His311 and Glu312 of 3zkd protein. Compound 11 with ethoxy group at R1 position interacted with Asn309 and Thr371 by hydrogen bonding followed by oxygen of ligand ethoxy group with Trp47. Alkyl group near X position interacted with Glu312 using H-bond. The best active site conformation from Autodock result the binding affinity of compound 11 with 3ZKD protein as -8.4 K Cal / mol. Similarly, H-bond interactions were predicted in compound 12 with the residues Asn309, His44, Arg40, Thr371, His311, Glu312 and Gln370 of 3zkd protein. Compound 12 display H-bonds near to R1 position with Arg40 and Thr371 followed by oxygen at X position interaction with His44. Asn309 interacted with piperazine N atom forming a favorable H-bond. Trifluoro group of compound 12 interacted well with Gly369. The best active site conformation from Autodock result the binding affinity of compound 12 with 3ZKD protein as -7.6 K Cal / mol.

Again, H-bond interactions were seen in compound 16 with the residues Asn309 and Trp47 of 3zkd protein. Compound 16 with ethoxy group at R1 position interacted with Asn309 and Thr371 by hydrogen bonding followed by H-bond of alkyl group near X position interacted with Glu312. Trifluoro group of compound 16 interacted well with Glu39 and Arg40. The best active site conformation from Autodock result the binding affinity of compound 16 with 3ZKD protein as -8.7 K Cal / mol. Similarly, H-bond interactions were predicted in compound 17 with the residues Asn309, Arg40, Thr371, His311 and Trp47 of 3zkd protein. Compound 17 display H-bonds near to R1 position with Trp47, Asn309 and Thr371. The best active site conformation from Autodock result the binding affinity of compound 17 with

3ZKD protein as -8.1 K Cal / mol. Further, H-bond interactions were predicted in compound 31 with the residues Asn309, Trp47, Glu312 and His44 of 3zkd protein. Compound 31 display Pi interactions with Arg40 and His311. The best active site conformation from Autodock result the binding affinity of compound 31 with 3ZKD protein as -8.3 K Cal / mol.

With various substituents at R, R1, X positions and keeping Y position fixed to N-ethyl group, designer series resulted few best leads based on PMIC values using QSAR final model. These leads were evaluated for H-bond interactions and binding scores using molecular docking studies. Residue interactions with His44, Trp47, Asn309 and His311 were common in almost all the designed compounds giving preference to H-bonding. The results were presented in **Table 4** with interacting residues, binding affinity scores from Autodock as well as PMIC values from QSAR final model. The results were favorable giving importance to model equation descriptors supporting QSAR studies. The molecular descriptors (weighted or unweighted) of obtained qsar model and type of molecular docking interactions (charged, hydrogen bond, dipole-dipole, van der Waals, pi-cation, etc.), were correlated and found to be in association with each other. RDF, WHIM and MoRSE descriptors weighted with Ionization potential, electronegativity indices were in relation to fluorine group charged interactions with arginine, histidine residues. The docking interactions of best compounds (Left image is compound 60 and Right image is compound 61) within 3ZKD active site from Discovery studio visualizer 2020 were depicted in **Figure 3**.

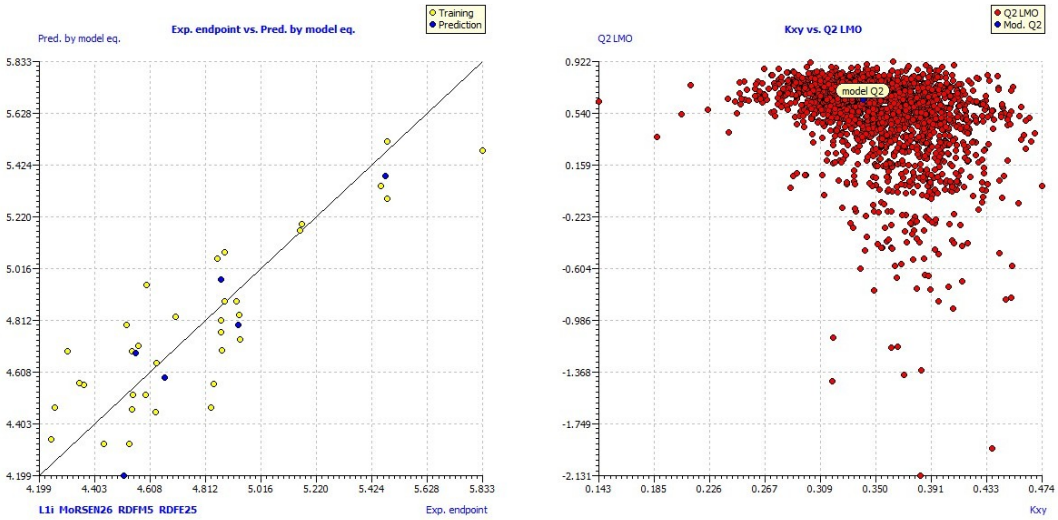

Figure 1: Scatter plot of dataset compounds using best model (left image) and LMO plot of best model located in the cluster of models attained (right image)

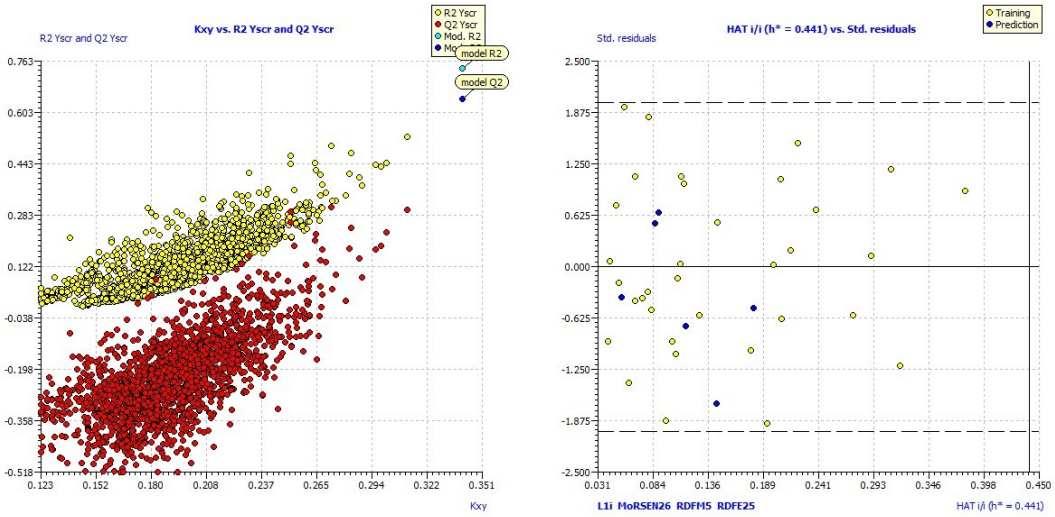

Figure 2: Y- Scrambles plot differentiating best model from scrambled models (left image) and Williams plot of best model showcasing dataset compounds within the standard deviation of 2.0 (right image)

Table 2: Residuals from model equation vs exp values

Name	pMIC	L1i	MoRSEN26	RDFM5	RDFE25	Pred activity by model eq	Residuals
1	4.542118	27.37518	-0.022	9.168	6.112	4.691201	-0.14908
2	4.874519	26.42734	-0.044	9.916	8.319	4.692949	0.18157
3	4.66314	27.23167	-0.037	8.899	5.267	4.588169	0.074971
4	4.365523	23.80416	-0.068	9.382	10.749	4.558691	-0.19317
5	4.842241	27.00802	-0.053	8.719	6.479	4.563059	0.279182
6	4.631527	26.14346	-0.032	9.949	6.388	4.645412	-0.01388
7	4.871278	26.86834	0.018	9.886	5.511	4.811267	0.060011
8	4.303207	26.65362	-0.066	9.824	9.938	4.688997	-0.38579
9	4.869345	25.3851	-0.067	10.96	12.221	4.767117	0.102228
10	4.936291	27.25877	0.044	12.764	0	4.831718	0.104573
11	5.488117	25.67033	0.005	10.614	6.539	4.784161	0.703956
12	5.531653	27.00011	-0.092	14.139	13.476	4.953814	0.577839
13	5.169411	24.23315	0.002	11.044	18.392	5.19238	-0.02297
14	4.594654	31.31839	-0.027	9.72	7.74	4.950932	-0.35628
15	4.885056	24.31077	-0.03	12.88	16.064	5.080001	-0.19495
16	5.832683	32.80132	-0.03	12.88	16.064	5.483302	0.349381
17	5.619789	25.48025	0.031	8.887	4.359	4.698291	0.921498
18	4.256725	26.57666	-0.054	11.346	1.625	4.467736	-0.21101
19	4.54607	25.16943	-0.059	11.927	4.37	4.518654	0.027416
20	4.439137	26.33789	-0.103	10.857	3.086	4.326187	0.11295
21	4.348141	24.59158	-0.05	10.644	6.945	4.56455	-0.21641
22	4.556737	25.62739	-0.085	10.462	11.949	4.684414	-0.12768
23	4.627825	24.79562	-0.023	8.019	4.564	4.451909	0.175916
24	4.59193	26.68537	-0.077	8.898	7.555	4.517242	0.074688
25	4.856049	32.39898	0.026	13.654	0	5.055676	-0.19963
26	4.93442	27.7299	-0.088	9.767	13.275	4.794705	0.139715
27	5.476254	31.25622	0.038	13.254	9.119	5.382968	0.093286
28	4.938925	30.72072	-0.164	14.415	9.293	4.735175	0.20375
29	4.869988	30.51179	-0.064	13.006	8.613	4.971908	-0.10192
30	4.88306	25.45354	-0.056	12.877	12.06	4.888586	-0.00553
31	5.481486	30.73019	0.033	13.863	12.9	5.517838	-0.03635
32	4.522445	29.9943	-0.154	12.823	12.635	4.793519	-0.27107
33	4.513145	25.48585	-0.074	9.447	0	4.197763	0.315382
34	4.24306	27.59835	-0.072	7.209	3.591	4.344293	-0.10123
35	4.832978	25.73579	-0.014	8.26	2.788	4.467975	0.365003
36	4.881074	28.0046	-0.132	10.781	1.931	4.258449	0.622625
37	5.114074	25.03785	-0.079	9.68	4.117	4.332433	0.781641
38	4.543027	27.18896	-0.075	9.343	4.807	4.459937	0.08309
39	4.530767	25.28917	-0.078	10.365	2.744	4.324887	0.20588
40	5.181115	27.59141	-0.05	9.21	7.738	4.672895	0.50822
41	4.565591	31.35294	0.027	5.042	2.441	4.712834	-0.14724

42	5.481486	33.76481	-0.049	11.259	13.563	5.292448	0.189038
43	5.160522	31.61604	0.058	11.498	3.468	5.164876	-0.00435
44	4.704433	34.76869	-0.097	11.11	4.805	4.826177	-0.12174
45	4.928118	27.51947	-0.002	10.973	7.144	4.888563	0.039555
46	5.458421	34.47656	-0.038	10.966	13.364	5.342202	0.116219

Table 3: Best designed compounds with QSAR model 4 predicted Mtb Gyrase B inhibitory activity

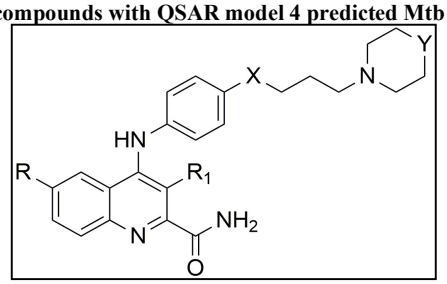

Name	R	R1	X	Y	L1i	MoRSEN26	RDFM5	RDFE25	pMIC
47	-OH	- p-fluoro phenyl	-S	-NC2H5	50.0636	-0.03	10.526	21.374	6.405132
48	-NO2	- p-hydroxy phenyl	-O	-NC2H5	49.4618	-0.136	13.144	28.024	6.399976
49	-CH3	- p-hydroxy phenyl	-O	-NC2H5	49.9071	-0.026	7.777	25.636	6.453775
50	-C2H5	- p-hydroxy phenyl	-O	-NC2H5	47.5355	-0.011	13.044	21.974	6.487671
51	-CH3	- p-hydroxy phenyl	-S	-NC2H5	47.9848	-0.113	14.121	29.466	6.508855
52	-NH2	- p-methoxy phenyl	-O	-NC2H5	52.0165	-0.1	13.868	24.528	6.538168
53	-NO2	- p-methoxy phenyl	-O	-NC2H5	51.8471	-0.134	12.936	26.694	6.458144
54	-NH2	- p-methoxy phenyl	-S	-NC2H5	54.5283	-0.06	11.824	18.976	6.480603
55	-CH3	- p-methoxy phenyl	-S	-NC2H5	53.9246	-0.099	11.629	22.676	6.457112
56	-OH	- p-methoxy phenyl	-S	-NC2H5	55.2092	-0.128	13.254	26.201	6.633183
57	-NO2	- p-methoxy phenyl	-O	-NCH3	47.7775	-0.054	18.399	18.294	6.453151

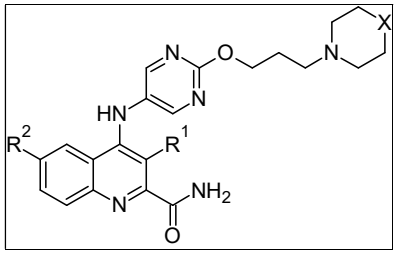

Name	R1	R2	X	L1i	MoRSEN26	RDFM5	RDFE25	pMIC
58	-Cl	-C6H5F	-NCH3	48.60043	-0.087	14.873	24.388	6.460118
59	-Cl	-tosyl	-NC2H5	33.13038	-0.028	15.331	37.554	6.464158

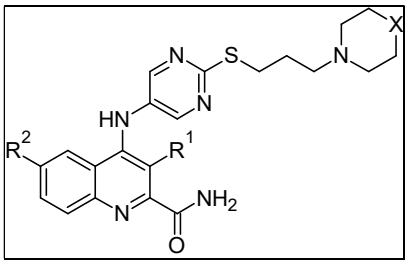

Name	R1	R2	X	L1i	MoRSEN26	RDFM5	RDFE25	pMIC
60	-H	-C6H5F	-NC2H5	52.47338	0.031	9.374	31.356	7.066353
61	-OH			52.56326	0.039	10.672	17.531	6.612123
62	-CH3	-tosyl	-NC2H5	53.57308	-0.001	13.493	12.369	6.450264

Table 4: Molecular docking results of designed compounds

Designed compounds	Binding energy (K Cal / mol)	Binding residue interactions along with distance (Å)
60	-9.2	Thr371 (2.8938), Arg193 (2.2034), Asn309 (2.313), Glu39 (2.988) and Hydrophobic interactions with His311, His44, Arg40
61	-8.6	Thr371 (2.7304), Arg193 (2.140), Asn309 (2.706), Glu39 (3.037), Thr189 (2.865) and Hydrophobic interactions with His311, His44, His43

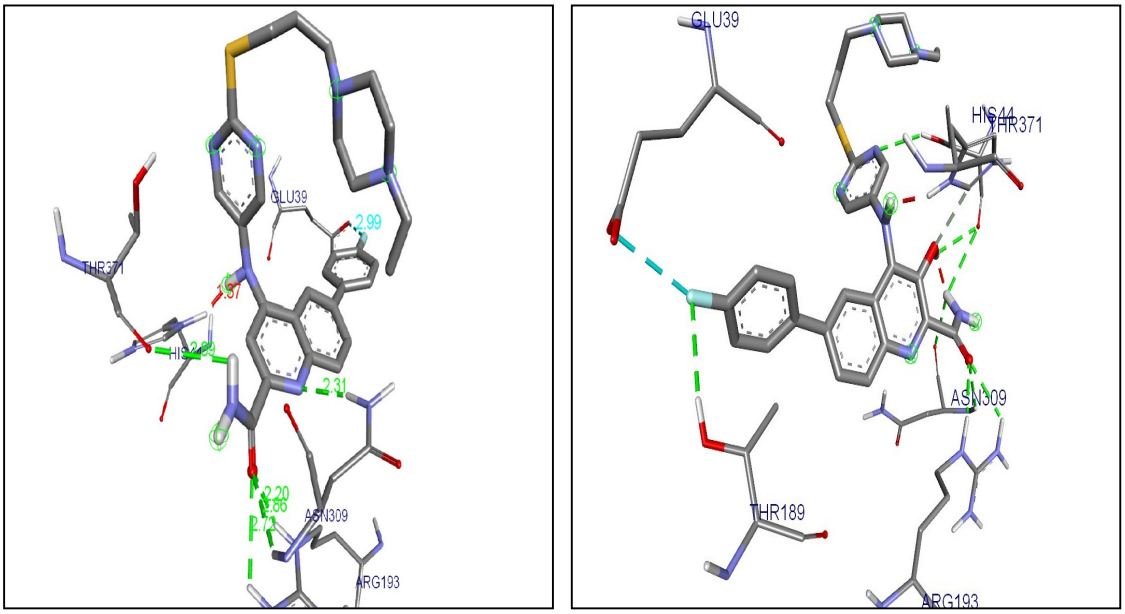

Figure 3: Docking interactions of compound 60 (Left image) and compound 61 (Right image) within 3ZKD: DNA Gyrase B active site

CONCLUSION

Current work aims towards identification and development of novel leads from a series of novel 4-aminoquinoline derivatives as inhibitors of Mtb DNA gyrase B using QSAR and molecular docking studies. QSAR model developed using WHIM, RDF and MoRSE based descriptors with both internal and external validated values established a meaningful relationship between structure and bioactivity of 4-aminoquinolines with Mtb Gyrase subunit B inhibitory activity. Positively correlated descriptors benefit the model along with leverage analysis. Utilizing molecular descriptors information from QSAR studies, a self explorative study on the dataset was performed to identify the model efficiency and accuracy. Further, structure bioactivity screening was performed to identify the role of various functional moieties on the core structure, which result a meaningful relationship between dataset compounds and DNA Gyrase B inhibitory activity. A series of compounds were designed from structure activity relationship information and tested for predicted bioactivity using QSAR model by obtaining molecular descriptor values from fore mentioned web servers. Best designed compounds having predicted bioactivity values above the dataset bioactivity values were considered for docking analysis to rule out hydrogen bond interactions. Docking results analyzed nonbonding interactions in the active site of

enzyme favouring hydrogen bond interactions with Thr189, Arg193, His44, Thr371, Asn309, Glu39 and His 311. Compound 42a with binding energy of -9.1 K Cal/mol have shown better predictions in both QSAR and molecular docking studies compared to compound 16 with binding energy of -8.7 K Cal/mol. Thus the present computational work reports the compound 42a as scaffold for the development of analogs to target 3zkd, DNA Gyrase B. The compound 42a has a good predicted potential of ~80nM MIC to inhibit DNA gyrase B and can be applied for further studies which aim to discover good therapeutic drugs.

CONFLICTS OF INTEREST: None

ACKNOWLEDGMENTS

We thank Prof. Gramatica P, University of Insubria, Italy for providing QSARINS software. We thank the Research Council of SRMIST and the Dean, SRM College of Pharmacy for support.

REFERENCES

[1] World Health Organization, Global tuberculosis report, 2019.

[2] Centers for disease control and prevention, Tuberculosis report, 2021.

[3] Lodish H, Berk A, Zipursky SL, Matsudaira P, Baltimore D, Darnell J, Molecular Cell Biology, 4th ed, W. H. Freeman, New York, 2000.

[4] Marko O, Miha K, Tom S, Discovery and Development of ATPase Inhibitors of DNA Gyrase as Antibacterial Agents, Curr Med Chem, 14(19), 2007, 2033–2047.

[5] Collin F, Karkare S, Maxwell A, Exploiting bacterial DNA gyrase as a drug target: current state and perspectives, Appl Microbiol Biotechnol, 92(3), 2011, 479-497.

[6] Barnard FM, Maxwell A, Interaction between DNA Gyrase and Quinolones: Effects of Alanine Mutations at GyrA Subunit Residues Ser83 and Asp87, Antimicrob Agents Chemother, 45(7), 2001, 1994-2000.

[7] Khan T, Sankhe K, Suvarna V, Sherje A, Patel K, Dravyakar B, DNA gyrase inhibitors: Progress and synthesis of potent compounds as antibacterial agents, Biomed Pharmacother, 103, 2018, 923–938.

[8] Chaudhari K, Surana S, Jain P, Patel HM, Mycobacterium Tuberculosis (MTB) GyrB inhibitors: An attractive approach for developing novel drugs against TB, Eur J Med Chem, 124, 2016, 160–185.

[9] Nayyar A, Malde A, Jain R, Coutinho E, 3D-QSAR study of ring-substituted quinoline class of anti-

tuberculosis agents, Bioorg Med Chem, 14(3), 2006, 847–856.

[10] Shanthakumar B, Kathiravan MK, Insights into structures of imidazo oxazines as potent polyketide synthase XIII inhibitors using molecular modeling techniques, J Recept Signal Transduct Res, 40, 2020, 313-323.

[11] Gopinath P, Kathiravan MK, QSAR and docking studies on Triazole Benzene Sulfonamides with human Carbonic anhydrase IX inhibitory activity, J Chemom, 33(12), 2019, e3189.

[12] Priya D, Kathiravan MK, Molecular insights into benzene sulphonamide substituted diarylpyrazoles as cyclooxygenase-2 inhibitor and its structural modifications, J Biomol Struct Dyn, 39(14), 2020, 5093–5104

[13] Srimathi R, Kathiravan MK, Lead optimization of 4-(thio)-chromenone 6-O-sulfamate analogs using QSAR, molecular docking and DFT – a combined approach as steroidal sulfatase inhibitors, J Recept Signal Transduct Res, 41, 2021, 123-137.

[14] Medapi B, Suryadevara P, Renuka J, Sridevi J P, Yogeeswari P, Sriram D, 4-Aminoquinoline derivatives as novel Mycobacterium tuberculosis GyrB inhibitors: Structural optimization, synthesis and biological evaluation, Eur J Med Chem, 103, 2015, 1-16.

[15] Spessard GO, ACD Labs/LogP dB 3.5 and ChemSketch 3.5, J Chem Inf Comput Sci, 38, 1998, 1250-1253.

[16] O'Boyle NM, Banck M, James CA, Morley C, Vandermeersch T, Hutchison GR, Open Babel: An open chemical toolbox, J Cheminform, 3, 2011, 33.

[17] Hanwell MD, Curtis DE, Lonie DC, Vandermeersch T, Zurek E, Hutchison GR, Avogadro: an advanced semantic chemical editor, visualization, and analysis platform. J. Cheminform, 4, 2012, 17.

[18] Dong J, Cao DS, Miao HY, Liu S, Deng BC, Yun YH, Wang NN, Lu AP, Zeng WB, Chen AF, ChemDes: an integrated web-based platform for molecular descriptor and fingerprint computation, J Cheminform, 7, 2015, 60.

[19] Gramatica P, Chirico N, Papa E, Cassani S, Kovarich S, QSARINS: A new software for the development, analysis, and validation of QSAR MLR models, J Comput Chem, 34(24), 2013, 2121–2132.

[20] Gramatica P, Cassani S, Chirico N, QSARINS-chem: Insubria datasets

and new QSAR/QSPR models for environmental pollutants in QSARINS, J Comput. Chem, 35, 2014, 1036–1044.

[21] Morris GM, Huey R, Lindstrom W, Sanner MF, Belew RK, Goodsell DS, Olson AJ, AutoDock4 and AutoDockTools4: Automated docking with selective receptor flexibility, J Comput Chem, 30(16), 2009, 2785–2791.

[22] Webb B, Sali A, Comparative Protein Structure Modeling Using MODELLER, Curr Protoc Bioinform, 54, 2016, 5.6.1-5.6.37.

[23] Discovery studio Visualizer Version 20.1.0.19295. BIOVIA, 2020.

[24] Consonni V, Ballabio D, Todeschini R, Evaluation of model predictive ability by external validation techniques, J. Chemom, 24(3), 2010, 194–201.

[25] Todeschini R, Gramatica P, New 3D Molecular Descriptors: The WHIM theory and QSAR Applications. Three-Dimensional Quantitative Structure Activity Relationships, Perspect drug discov des, 9, 1998, 355–380.